Jiang, Song; Hou, Peng Xiang; Chen, Mao Lin; Wang, Bing Wei; Sun, Dong Ming; Tang, Dai Ming; Jin, Qun; Guo, Qing Xun; Zhang, Ding Dong; Du, Jin Hong; Tai, Kai Ping; Tan, Jun; Kauppinen, Esko I.; Liu, Chang; Cheng, Hui Ming

Ultrahigh-performance transparent conductive films of carbon-welded isolated single-wall carbon nanotubes

Published in:
Science Advances

DOI:
10.1126/sciadv.aap9264

Published: 04/05/2018

Document Version
Publisher's PDF, also known as Version of record

MATERIALS SCIENCE

Ultrahigh-performance transparent conductive films of carbon-welded isolated single-wall carbon nanotubes

Song Jiang,[1,2,3,4]* Peng-Xiang Hou,[1,5]* Mao-Lin Chen,[1,5] Bing-Wei Wang,[1,4] Dong-Ming Sun,[1,5] Dai-Ming Tang,[1,5] Qun Jin,[1,4] Qing-Xun Guo,[6] Ding-Dong Zhang,[1,5] Jin-Hong Du,[1,5] Kai-Ping Tai,[1,5] Jun Tan,[1,5] Esko I. Kauppinen,[7] Chang Liu,[1,5†] Hui-Ming Cheng[1,2,5,8†]

Single-wall carbon nanotubes (SWCNTs) are ideal for fabricating transparent conductive films because of their small diameter, good optical and electrical properties, and excellent flexibility. However, a high intertube Schottky junction resistance, together with the existence of aggregated bundles of SWCNTs, leads to a degraded optoelectronic performance of the films. We report a network of isolated SWCNTs prepared by an injection floating catalyst chemical vapor deposition method, in which crossed SWCNTs are welded together by graphitic carbon. Pristine SWCNT films show a record low sheet resistance of 41 ohm $\square^{-1}$ at 90% transmittance for 550-nm light. After HNO_3 treatment, the sheet resistance further decreases to 25 ohm $\square^{-1}$. Organic light-emitting diodes using this SWCNT film as anodes demonstrate a low turn-on voltage of 2.5 V, a high current efficiency of 75 cd A^{-1}, and excellent flexibility. Investigation of isolated SWCNT-based field-effect transistors shows that the carbon-welded joints convert the Schottky contacts between metallic and semiconducting SWCNTs into near-ohmic ones, which significantly improves the conductivity of the transparent SWCNT network. Our work provides a new avenue of assembling individual SWCNTs into macroscopic thin films, which demonstrate great potential for use as transparent electrodes in various flexible electronics.

INTRODUCTION

Transparent conductive films (TCFs) are an important component of various optoelectronic devices such as touch screens, smart windows, liquid crystal displays, organic light-emitting diodes (OLEDs), and organic photovoltaic cells (*1*). Indium tin oxide (ITO) has been the most widely used transparent conductive material with good electrical and optical properties; however, the limited reserves of indium and the brittle nature of ITO hinder its sustainable application in flexible electronics. With the emerging and rapid development of flexible electronic devices, alternative transparent conductive materials with good flexibility have been investigated, including carbon nanotubes (CNTs) (*2*–*4*), graphene (*5*), metal nanowires (*6*), metal meshes (*7*), conducting polymers (*8*), and various hybrids (*9*, *10*). Among them, single-wall CNTs (SWCNTs) are an appealing candidate because of their good electrical conductivity, high structural stability, excellent flexibility, and desirable optical properties such as low refractive index, little coloration, and low haze (*11*). In the past decades, significant effort has been dedicated to obtaining high-performance SWCNT-based TCFs using both wet (*2*, *12*) and dry processes (*13*, *14*). However, the performance of SWCNT TCFs is still not as good as ITO and falls far short of what might be expected from the electrical and optical properties of individual SWCNTs (*15*). For example, the sheet resistances of ITO on rigid and flexible substrates are ~10 ohm $\square^{-1}$ (*16*) and ~30 ohm $\square^{-1}$ (*17*), respectively, at 90% transmittance for 550-nm light, whereas values for pristine SWCNT TCFs (without doping or patterning) are usually above 200 ohm $\square^{-1}$ (*18*, *19*). Junction resistance and bundling are recognized as the two major issues accounting for the poor performance of SWCNT TCFs. It is known that the junction resistance between nanotubes is much higher than the intrinsic tube resistance, and the electrical conductivity of a CNT TCF is largely dominated by the resistance at intertube junctions (*20*, *21*). Furthermore, SWCNTs synthesized by conventional methods are usually a mixture of ~1/3 metallic (m-) and ~2/3 semiconducting (s-) SWCNTs. Therefore, ~4/9 of intertube junctions are dominated by Schottky barriers (*20*, *22*), which greatly suppress carrier transport and increase junction resistance. On the other hand, as-prepared SWCNTs often aggregate into bundles that contribute little to the electrical conductivity but lower the light transmission (*15*). There is, therefore, a need to fabricate SWCNT networks containing only small bundles or isolated nanotubes with ohmic contacts to achieve optimized transmittance and conductivity. However, because of the small size and strong van der Waals interaction of SWCNTs and the difficulty of synthesizing pure m- or s-SWCNTs, there remains a big challenge to control the percentage of isolated tubes and the structure of junctions in an SWCNT network.

Here, we report a network consisting of carbon-welded isolated SWCNTs with near-ohmic joint contacts. The isolated SWCNTs permit maximum light transmission, whereas the carbon-welded junctions efficiently decrease the electrical resistance. By using an injection floating catalyst chemical vapor deposition (injection FCCVD) method, high-quality (I_G/I_D = 175), large-mean diameter (~2.0 nm) isolated SWCNTs were prepared. Large-area SWCNT TCFs (80 mm × 80 mm) were fabricated by gas phase filtration involving no liquid phase processes. All these characteristics give the as-prepared TCFs a very low sheet resistance (R_s) of 41 ohm $\square^{-1}$ at 90% transmittance (T) for 550-nm light, which is about 5.5 times lower than that of the best reported undoped CNT TCF (*18*). After HNO_3 doping, the resistance was further decreased to 25 ohm $\square^{-1}$, even better than that of ITO supported on a flexible substrate (*17*). Studies on isolated SWCNT-based field-effect transistors (FETs) show that the joints between nanotubes convert what would be Schottky contacts between m-SWCNTs and s-SWCNTs into near-ohmic ones and, hence, markedly improve the electrical conductivity of the

[1]Shenyang National Laboratory for Materials Science, Institute of Metal Research, Chinese Academy of Sciences, Shenyang 110016, China. [2]School of Physical Science and Technology, ShanghaiTech University, Shanghai 200031, China. [3]State Key Laboratory of Functional Materials for Informatics, Shanghai Institute of Microsystem and Information Technology, Chinese Academy of Sciences, Shanghai 200050, China. [4]University of Chinese Academy of Sciences, Beijing 100049, China. [5]School of Materials Science and Engineering, University of Science and Technology of China, Shenyang 110016, China. [6]State Key Laboratory of Polymers Physics and Chemistry, Changchun Institute of Applied Chemistry, Chinese Academy of Sciences, Changchun 130022, China. [7]Aalto University School of Science, Department of Applied Physics, PO Box 15100, FI-00076 Aalto, Espoo, Finland. [8]Tsinghua-Berkeley Shenzhen Institute, Tsinghua University, Shenzhen 518055, China.
*These authors contributed equally to this work.
†Corresponding author. Email: cliu@imr.ac.cn (C.L.); cheng@imr.ac.cn (H.-M.C.)

SWCNT network. In addition, flexible OLEDs using a pristine SWCNT film as anodes show an outstanding optoelectronic performance and excellent flexibility. The maximum current and power efficiencies are 75 cd A^{-1} and 89.5 lumens (lm) W^{-1}, respectively, which are the best to date for CNT-based OLEDs and comparable to those of ITO-based OLEDs.

RESULTS

Synthesis and characterization of isolated SWCNT networks with carbon-welded joints

SWCNTs were synthesized using an injection FCCVD method (*23*) using hydrogen (H_2) as a carrier gas. Surplus carbon has usually been considered undesirable for SWCNT synthesis (*24*), but here, it is seen to have a beneficial effect. Detailed preparation procedures are described in Materials and Methods, and a schematic of the injection FCCVD system is shown in fig. S1. Figure 1A shows a typical transmission electron microscopy (TEM) image of the SWCNT network. We can see that the network is composed of isolated SWCNTs with carbon-welded junctions (Fig. 1A and fig. S2A). The percentage of carbon-welded junctions is estimated to be ~98%, based on TEM observations of more than 400 intertube junctions. Compared to the growth of normal samples composed of entangled SWCNT bundles (fig. S2, B and C), the key factor for growing carbon-welded isolated SWCNTs is to control the H_2 flux. By using a high-flux H_2 carrier gas, catalyst precursor (ferrocene), growth promoter (thiophene), and carbon source (ethylene and toluene) concentrations are decreased, which result in fewer nuclei for SWCNTs in a specific volume. A second factor is that the residence time of gas in the high-temperature zone decreases, which shortens the growth time of SWCNTs. As a consequence, the number and length of SWCNTs in the reactor are decreased, which greatly suppresses bundle formation induced by the van der Waals force between adjacent SWCNTs during growth (*3*). On the other hand, the surplus carbon atoms by the pyrolysis of hydrocarbons deposit as graphitic carbon, just like the growth of vapor phase–grown carbon fibers (*25*), preferentially at SWCNT junctions forming the carbon welding and preventing bundling of SWCNTs by van der Waals force. Thus, isolated SWCNTs with carbon-welded junctions can be obtained. Furthermore, the isolated nanotubes have a large mean diameter of ~2.0 nm and straight tube walls. The percentage of isolated nanotubes and the diameters of the SWCNTs were measured under TEM, and the results are shown in Fig. 1B and fig. S3A. Observations of 253 nanotubes/bundles suggest that 85% of the filaments in the network are isolated nanotubes, whereas the rest are

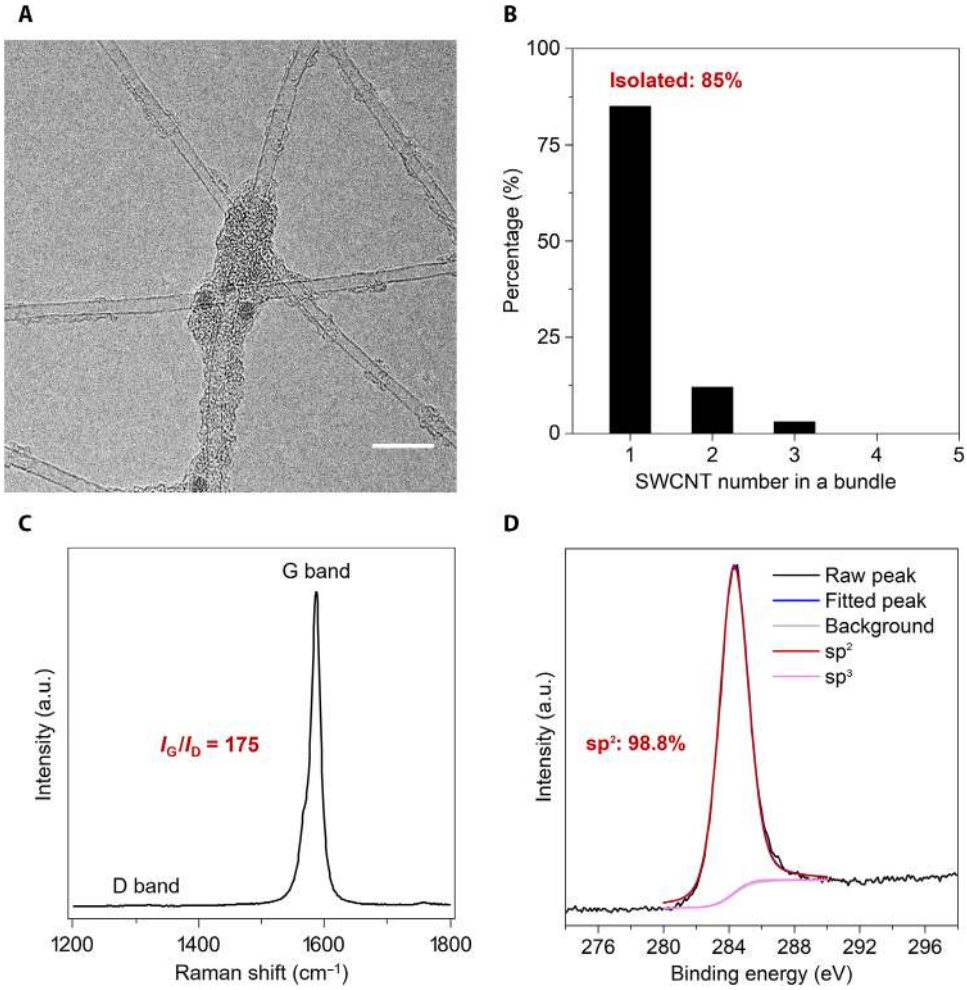

Fig. 1. Microstructures of isolated SWCNTs with carbon-welded joints. (**A**) Typical TEM image. Scale bar, 10 nm. (**B**) Statistical data of the numbers of isolated and bundled SWCNTs in the network. (**C**) Raman spectrum excited by a 633-nm laser. (**D**) C 1s XPS spectrum. a.u., arbitrary units.

two- or three-tube small bundles (Fig. 1B). Measurements of 120 isolated SWCNTs (fig. S3A) show that their diameters are distributed in the 1.4 to 2.4 nm range with a mean diameter of ~2.0 nm.

As mentioned above, the SWCNT network is composed of isolated SWCNTs that are somehow welded together by surplus carbon at their junctions. High-resolution spherical aberration (Cs)–.corrected TEM characterization was performed to further characterize the structure of surplus carbon. As shown in fig. S3B, both the carbon and SWCNT showed a lattice-resolved structure, and the interlayer spacing of the carbon is ~0.33 nm, suggesting the existence of graphitic carbon. A typical laser Raman spectrum of the network sample (Fig. 1C) shows a very high G band and an almost invisible D band with a I_G/I_D value of 175 for a 633-nm laser, indicative of a well-crystallized sp^2 C-C structure (*26*), which are further confirmed by 532- and 785-nm laser Raman spectra with high I_G/I_D (fig. S3C). Moreover, the content of the sp^2 carbon of the network is determined to be 98.8% by x-ray photoelectron spectroscopy (XPS) measurements, as shown in Fig. 1D. These results indicate that the sp^2 C-C structure accounts for the overwhelming majority of the sample, which is further supported by local electron energy-loss spectroscopy (EELS) at the C *K*-edge in scanning transmission electron microscopy (STEM). As shown in fig. S3 (D to F) of STEM-EELS, the spectrum profiles of the SWCNTs and the carbon welding are similar to that of graphite in terms of three characteristic peaks (~285, 292, and 300 eV) of C *K*-edge, especially as evidenced by a sharp σ* peak at ~292 eV (*27*), whereas that of the amorphous carbon on a Cu grid shows a broad σ* peak. We heat-treated pristine samples in air at temperatures ranging from 400° to 800°C for 30 min and checked their structural changes under TEM (fig. S4). Even after harsh oxidation treatment at 700°C, the structure of the carbon welding and SWCNTs remained almost unchanged (fig. S4D). When the temperature was further increased to 750°C, most SWCNTs were destroyed but the carbon welds survived (fig. S4E). When the treatment temperature was increased to 800°C, both the SWCNTs and carbon welds were completely removed. These results further confirm that the carbon welding material is mainly composed of sp^2-bonded graphitic carbon rather than amorphous carbon.

A scanning electron microscopy (SEM) image (Fig. 2A) of the as-prepared SWCNTs on a SiO_2/Si substrate shows a random SWCNT network consisting of straight and long SWCNTs. Measurements of 235 SWCNTs based on SEM images (Fig. 2, B and C) indicate a mean

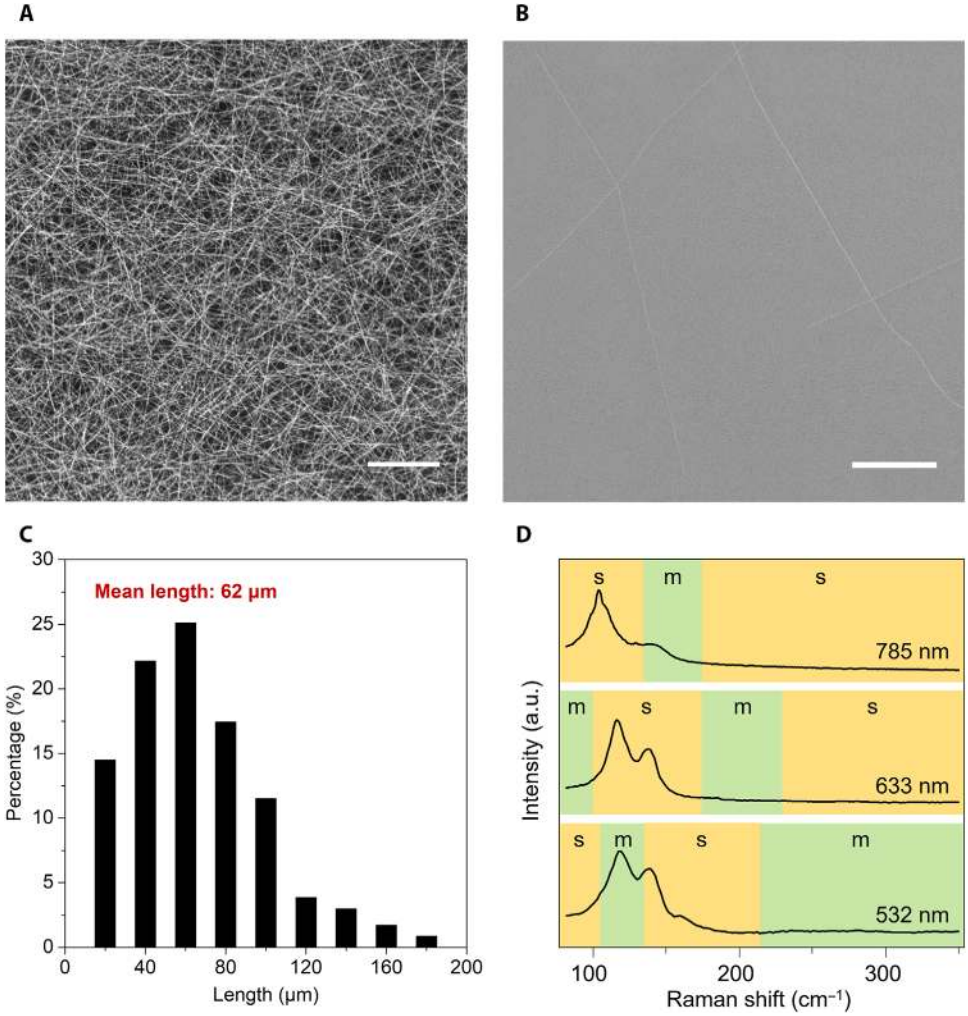

Fig. 2. SEM images, length distribution, and Raman spectra of the SWCNTs. (**A** and **B**) SEM images of SWCNT networks on SiO_2/Si wafers transferred from filter membranes with collection times of 10 min and 5 s, respectively. Scale bars, 0.5 μm (A) and 10 μm (B). (**C**) Length distribution of the SWCNTs measured by SEM. (**D**) RBM mode Raman spectra of the SWCNTs excited by 532-, 633-, and 785-nm lasers.

tube length of ~62 μm, and the longest length observed is ~190 μm. These long SWCNTs would facilitate carrier transfer in the network because of fewer intertube junctions. Raman spectra of the carbon-welded SWCNT network excited by 532-, 633-, and 785-nm lasers show narrow radial breathing mode (RBM) peaks ranging from 105 to 145 cm^{-1} (Fig. 2D), where the peaks originating from metallic and semiconducting SWCNTs are highlighted according to the classical Kataura plot (see Materials and Methods). It can be seen that both semiconducting and metallic SWCNTs coexist in the sample, which is further confirmed by absorption spectrum (fig. S4F). The diameters calculated from the RBM peaks (*28*) are in the 1.7 to 2.6 nm range, which is consistent with TEM observations.

SWCNT TCFs

We fabricated SWCNT TCFs using the as-prepared samples by a dry filtration and transfer process (*13*). The SWCNTs synthesized by the injection FCCVD method flowed with the carrier gas to the downstream of the reactor, where a porous cellulose filter membrane was installed (fig. S5A) and the SWCNTs were deposited (fig. S5B). The SWCNT network was then transferred to polyethylene terephthalate (PET) by simple pressing, followed by ethanol densification of the SWCNT film (see Materials and Methods). As shown in Fig. 3A and fig. S5C, a uniform and large-area TCF (80 mm × 80 mm) was obtained. To evaluate the uniformity of the film, we divided it into 16 parts of the same size and measured the R_s and T of each part (fig. S5C). As shown in fig. S5 (C and D), a mean R_s of 163 ohm $\square^{-1}$ at 96.9% T was obtained, with maximum R_s and T deviations of 4.3 and 0.4%, respectively. They indicate a good structural uniformity of the SWCNT network. T versus R_s is plotted in Fig. 3B and tabulated in table S1A, together with the results for previously reported SWCNT TCFs in the literature (*4*, *14*, *15*, *18*, *29*, *30*) and that of a superior ITO TCF on a polymer substrate (*17*). The average R_s of our SWCNT TCFs is 41 ohm $\square^{-1}$ at 90% T for 550-nm light, about 5.5 times lower than that of the best value previously reported (*18*) and very close to that of ITO TCF. Moreover, the changes of R_s with T of our samples almost follow the theoretical T versus R_s curve (*31*). This high performance can meet the demands of most commercial applications including touch screens, smart windows, liquid crystal displays, and OLEDs (*32*). After HNO_3 doping, the R_s of the SWCNT TCF further decreased to 25 ohm $\square^{-1}$, much lower than all results for previously reported doped CNT TCFs in the literature (*2*–*4*, *12*, *14*, *33*), even better than that of ITO supported on a flexible substrate (Fig. 3C and table S1B) (*17*). It is worth mentioning that the R_s of our sample decreased only by 1.6 times after HNO_3 doping, which is much lower than values reported in the literature (*21*). HNO_3 may play two roles upon treatment of SWCNT thin films: thickness decrease by the removal of adsorbates and chemical doping through charge transfer (*34*). For our SWCNT TCFs prepared by a dry filtration and transfer process, we believe that the main effect of HNO_3 treatment is chemical doping, which results in decreased tube-tube junction resistance and decreases the R_s of SWCNT TCFs more than three times (*21*). This result confirms that the unique carbon-welded joints of our SWCNT film effectively decrease the tube-tube junction resistance. A comparative experiment was performed by synthesizing bundled SWCNT films without the carbon-welded joints using the same injection FCCVD technique (for details, see Materials and Methods and fig. S1). The performance of the TCFs obtained is shown in fig. S6A, where it can be seen that bundled SWCNT TCFs without the carbon-welded joints have inferior optoelectronic performance, with an R_s at 90% T that is 6.6 times higher than the isolated SWCNT TCFs with the carbon-welded joints. Considering the similar synthesis method used and the similar characteristic structures of SWCNTs obtained including tube diameter and I_G/I_D value (fig. S6, B and C), the superior optoelectronic performance (fig. S6A) of the isolated SWCNT TCFs can reasonably be ascribed to the isolated SWCNTs and the unique carbon-welded joints between them. It is known that carrier transport mainly occurs along the outermost layer of a nanotube bundle, leaving the bundle core as "dead mass" that only contributes to optical absorption (*35*). Here, the fact that 85% of the SWCNTs are isolated greatly decreases the dead mass buried in bundles, which leads to the excellent transmittance of the TCFs. The carbon-welded joints consist of graphitic carbon with an overwhelming proportion of sp^2 bonding, and this greatly improves the electrical transport between crossed nanotubes. Thus, the TCFs composed of isolated SWCNTs show not only very little optical absorption but also high electrical conductivity.

Good chemical stability and mechanical durability are critical for the components of flexible devices. Figure 3D shows the changes in R_s of the pristine and HNO_3-doped SWCNT TCFs put in ambient air for over 20 months. It can be seen that the R_s value is very stable with less than 2% variation for the pristine SWCNT TCF. On the other hand, the R_s of the HNO_3-doped TCF is unstable, a great increase in R_s is observed after 1 month due to HNO_3 desorption (*36*), after which the value is gradually stabilized at ~36 ohm $\square^{-1}$. In addition, we examined the stability of the TCF using an accelerated aging test (250 hours at 60°C and 90% relative humidity), which is a requirement for commercial transparent electrodes (*36*). As shown in table S2, the SWCNT TCF demonstrated excellent resistance to the chemical corrosion, showing a very small R_s decrease of 7%. This excellent chemical stability is ascribed to both the good intrinsic corrosion resistance of the SWCNTs and the tight tube-tube welding. We also investigated the mechanical durability of the SWCNT TCFs by measuring the R_s changes after different bending cycles and angles (fig. S6, D and E). As shown in Fig. 3E and fig. S6 (D and E), the films were bent to an angle of 70° and a minimum radius of curvature of 5 mm. No conductance degradation was observed even after 4000 bending cycles, which indicates excellent mechanical durability. After 10,000 bending cycles, the R_s increased slightly by 9%. In contrast, the R_s increase of commercial ITO-PET films rapidly doubled after only 200 bending cycles and increased 18-fold after 1000 bending cycles. Besides, the performance of the SWCNT TCF is almost stable with bending angles from 0° to 180° (Fig. 3F). However, the R_s of commercial ITO-PET films increases almost exponentially. These results firmly prove the excellent chemical stability and mechanical durability of our SWCNT TCFs. We note that, for real application of the SWCNT TCFs, processing issue, which may be different from that of traditional ITO TCFs, should also be addressed.

OLEDs with SWCNT TCF anodes

To verify the performance of our SWCNT TCFs, we fabricated flexible phosphorescent green OLEDs using an as-produced SWCNT TCF (69 ohm $\square^{-1}$, 92.7% T for 550-nm light) as anodes. Figure S7A schematically shows the structure of the SWCNT OLEDs on a flexible PET substrate. Figure 4A shows the optical image of a lit SWCNT OLED with an approximately 5-V voltage supply, which demonstrates bright and uniform green phosphorescence. Figure 4B shows the electroluminescent performance of the OLED, with a maximum luminance of 4088 cd m^{-2} and a turn-on voltage of 2.5 V, one of the lowest values in the literature (*37*). This low turn-on voltage is attributed to the high optoelectronic performance of our SWCNT TCF. Current efficiency and power efficiency versus luminance are shown in Fig. 4C. The maximum current and

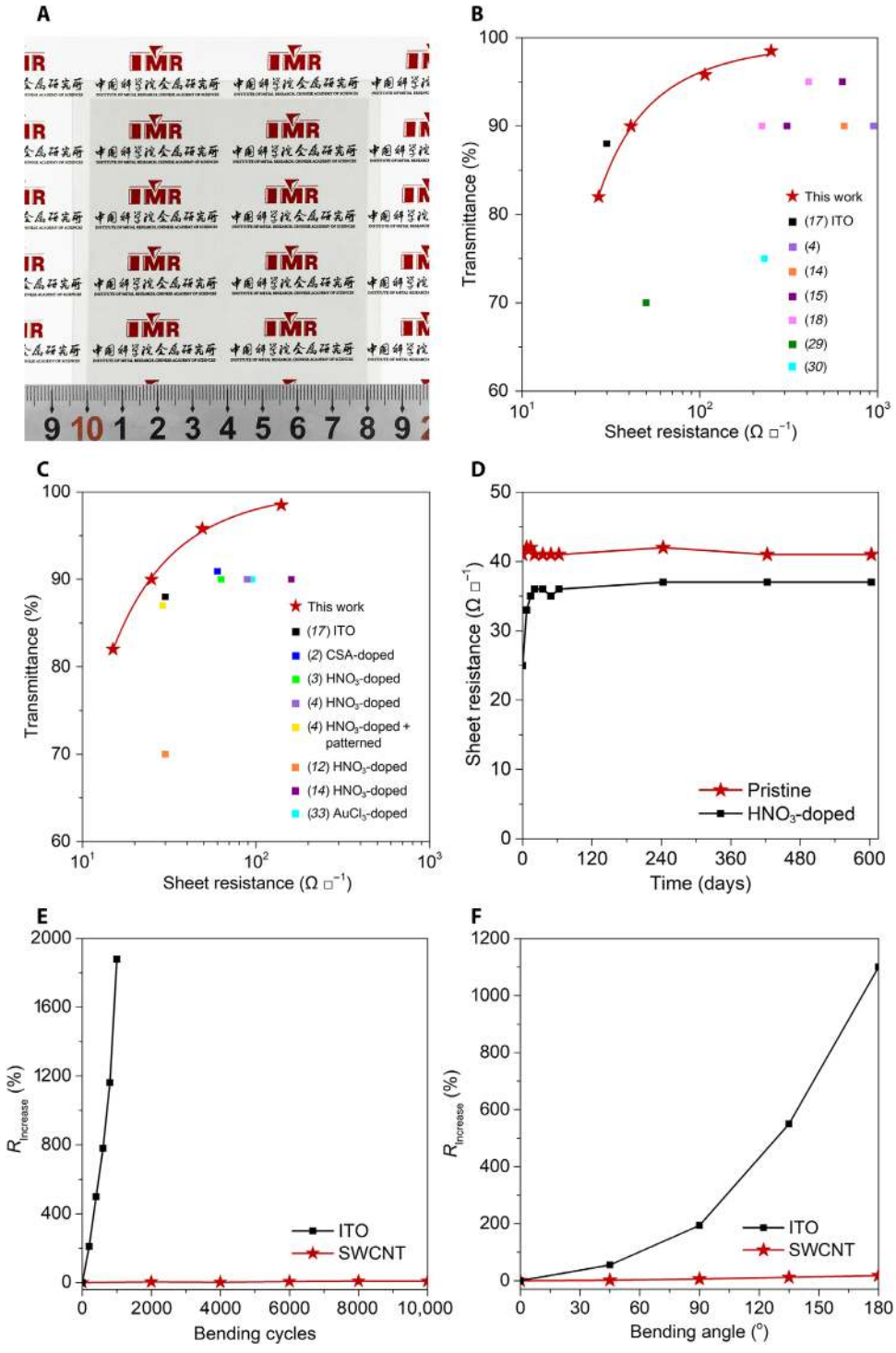

Fig. 3. Performance of SWCNT TCFs. (**A**) Optical image of an 80 mm × 80 mm SWCNT TCF. (**B**) *T* (for 550-nm light) versus R_s of our SWCNT TCFs together with the previously reported results for untreated CNT TCFs in the literature (*4*, *14*, *15*, *18*, *29*, *30*) and a superior ITO TCF on a polymer substrate (*17*). (**C**) *T* (for 550-nm light) versus R_s of our doped SWCNT TCFs together with the reported results for doped CNT TCFs in the literature (*2*–*4*, *12*, *14*, *33*) and the superior ITO TCF (*17*). For our SWCNT TCFs in (B) and (C), the R_s was measured at least four different points for every TCF, and the maximum R_s deviation for specific *T* is below 6% by performing three or four experiments. (**D**) Variations in R_s of the pristine and the HNO_3-doped SWCNT TCFs exposed to ambient air for over 20 months. (**E**) Variations in R_s of the SWCNT and the commercial ITO-PET TCFs as a function of the cycles of bending to a radius of 5 mm. (**F**) Variations in R_s versus bending angle for the SWCNT and the commercial ITO-PET TCFs.

power efficiencies are 75 cd A^{-1} and 89.5 lm W^{-1}, respectively, where the current efficiency is 7.5 times higher than the best reported value for SWCNT anode–based OLEDs in the literature (*37*–*39*) and outperforms the best value of a reported ITO-PET OLED (Fig. 4D) (*40*). Furthermore, the SWCNT OLED shows an excellent external quantum efficiency of over 15% (fig. S7B). Bending tests were further performed to investigate the performance of bended OLED devices. It was found that the luminance of the OLED decreased by ~10% at a high bending angle of 140° with a minimum curvature radius of ~2 mm (fig. S7C). At a bending angle of 70° and a minimum curvature radius of ~4 mm, the luminance decreased within 10% after 800 cycles (fig. S7D). A dynamic demonstration was shown in movie S1. All results of bending tests exhibit that our SWCNT OLEDs have reliable performance and good flexibility. It is worth noting that the overall performance can be further improved if the devices are packaged so that the effects of oxygen and humidity in air are avoided. Therefore, these results demonstrate that our SWCNT TCFs hold great promise for use in flexible OLED devices.

SWCNT FETs

To further reveal the effect of the carbon welding on the transport properties of crossed SWCNTs, we constructed FETs using crossed SWCNTs without and with the carbon-welded joints, and the typical layouts of the FETs are shown in Fig. 5 (A and C). Atomic force microscopy (AFM) characterization showed that there is no carbon welding at the intertube junction in Fig. 5A, whereas the two SWCNTs in Fig. 5C are welded together (insets of Fig. 5, A and C). We then determined the electrical type, that is, semiconducting or metallic, of each SWCNT based on the transfer characteristics of the FETs. The results indicate that, in both Fig. 5 (A and C), there is one m-SWCNT and one s-SWCNT (fig. S8, A and B).

We also studied the electrical conduction between crossed m-SWCNTs and s-SWCNTs. As can be seen in Fig. 5B, an obvious nonlinear curve of m-s drain current (I_{ds}) versus drain voltage (V_{ds}) is observed. It is well known that crossed m-SWCNTs and s-SWCNTs with diameters over 1 nm usually behave like a Schottky diode that shows a nonlinear and asymmetric I_{ds}-V_{ds} curve owing to the existence of a Schottky barrier at the tube-tube junction (*20*, *22*). Our SWCNTs have a mean diameter of ~2.0 nm (fig. S3A); thus, the nonlinear and asymmetric I_{ds}-V_{ds} curve of the crossed m-SWCNTs and s-SWCNTs is consistent with previous reports. However, surprisingly, for the carbon-welded m-SWCNTs and s-SWCNTs, near-linear and symmetric behavior of the m-s I_{ds} versus V_{ds} curve is observed (Fig. 5D), especially in the low voltage range (inset of Fig. 5D). This near-linear and symmetric behavior indicates near-ohmic contact at the m-SWCNT/s-SWCNT junction. Because the SWCNTs in Fig. 5 (A and C) have similar diameters, the abnormal phenomena observed are attributed to the unique carbon-welded joint, which effectively reduces the Schottky barrier between m-SWCNTs and s-SWCNTs due to the similar work functions of carbon materials

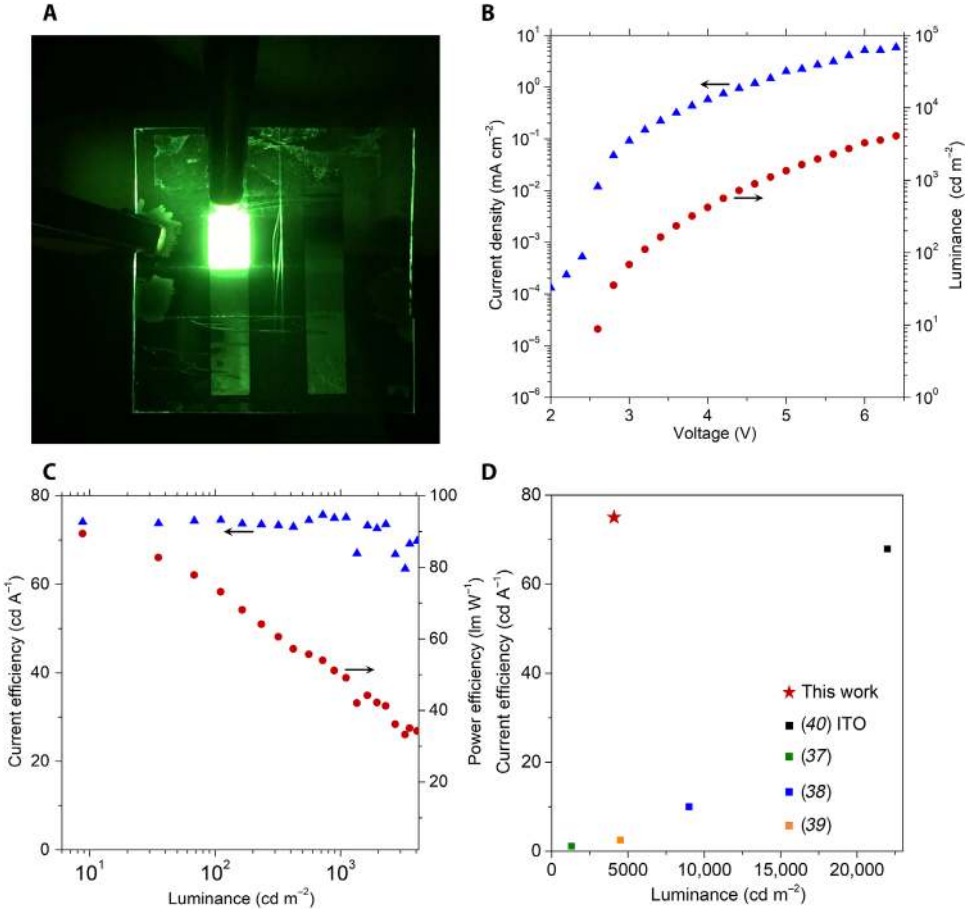

Fig. 4. Phosphorescent green SWCNT OLED and its performance. (**A**) Optical image of a lit SWCNT OLED. (**B**) Current density and luminance versus voltage. (**C**) Current efficiency and power efficiency versus luminance. (**D**) A comparison of the current efficiency and luminance of our SWCNT OLED with those of the previously reported CNT anode–based OLEDs in the literature (*37*–*39*) and the best ITO-PET OLED (*40*).

(*41*, *42*). The "carbon welding" is composed of graphitic nanosheets with different sizes and edge structures that have different energy bands (*43*). Therefore, the carbon-welded joint at the m-SWCNT/s-SWCNT junction may provide a moderate Fermi level to effectively convert one high Schottky barrier into two lower Schottky barriers (fig. S8, C and D). Furthermore, the carbon welding possibly also functions to protect the tube-tube junction from oxygen doping, which can reduce the Fermi level difference of m-SWCNTs and s-SWCNTs and lead to a further decrease of the Schottky barrier. As a result, the carbon-welded m-SWCNTs and s-SWCNTs show near-ohmic contact. In addition, the carbon welding can greatly promote tunneling at the m-SWCNT/s-SWCNT junction due to the increased contact area and more conducting channels. Therefore, the current is much higher in the low voltage range compared with a normal m-SWCNT/s-SWCNT Schottky device (*20*). The transformation from Schottky contact of m-SWCNT/s-SWCNT junctions into near-ohmic contact and the stronger tunneling induced by the carbon welding significantly improve the electrical conductivity of the SWCNT TCFs. As for the m-SWCNT/m-SWCNT and s-SWCNT/s-SWCNT junctions, the carbon welding can also greatly increase the carrier transport because of stronger tunneling. In addition, our SWCNTs have a long mean length (~62 μm), a large mean diameter (~2.0 nm), and good crystallinity (I_G/I_D = 175). All these structural characteristics contribute to the excellent optoelectronic performance, chemical stability, and mechanical durability of the SWCNT TCFs.

DISCUSSION

We have synthesized a unique carbon-welded network of isolated SWCNTs with near-ohmic joint contacts using an injection FCCVD method. An untreated SWCNT TCF has a record low R_s of 41 ohm $\square^{-1}$ at 90% T for 550-nm light and has excellent uniformity, chemical stability, and flexibility. R_s was further decreased to 25 ohm $\square^{-1}$ at 90% T by HNO_3 doping. This ultrahigh optoelectronic performance is mainly ascribed to the unique carbon-welded joints and the isolated SWCNTs. The carbon-welded joints play roles in both decreasing the tube-tube junction resistance by converting the Schottky contacts between m-SWCNTs and s-SWCNTs into near-ohmic ones and preventing the formation of bundles. The isolated SWCNTs provide efficient carrier transfer pathways with no dead mass while leading to very little optical absorption. OLEDs were fabricated using the SWCNT TCF as anodes, and excellent overall performance in terms of current efficiency, luminance, and flexibility was demonstrated. The simple and scalable production process, excellent optoelectronic performance, good chemical stability, and desirable mechanical durability of the SWCNT TCFs

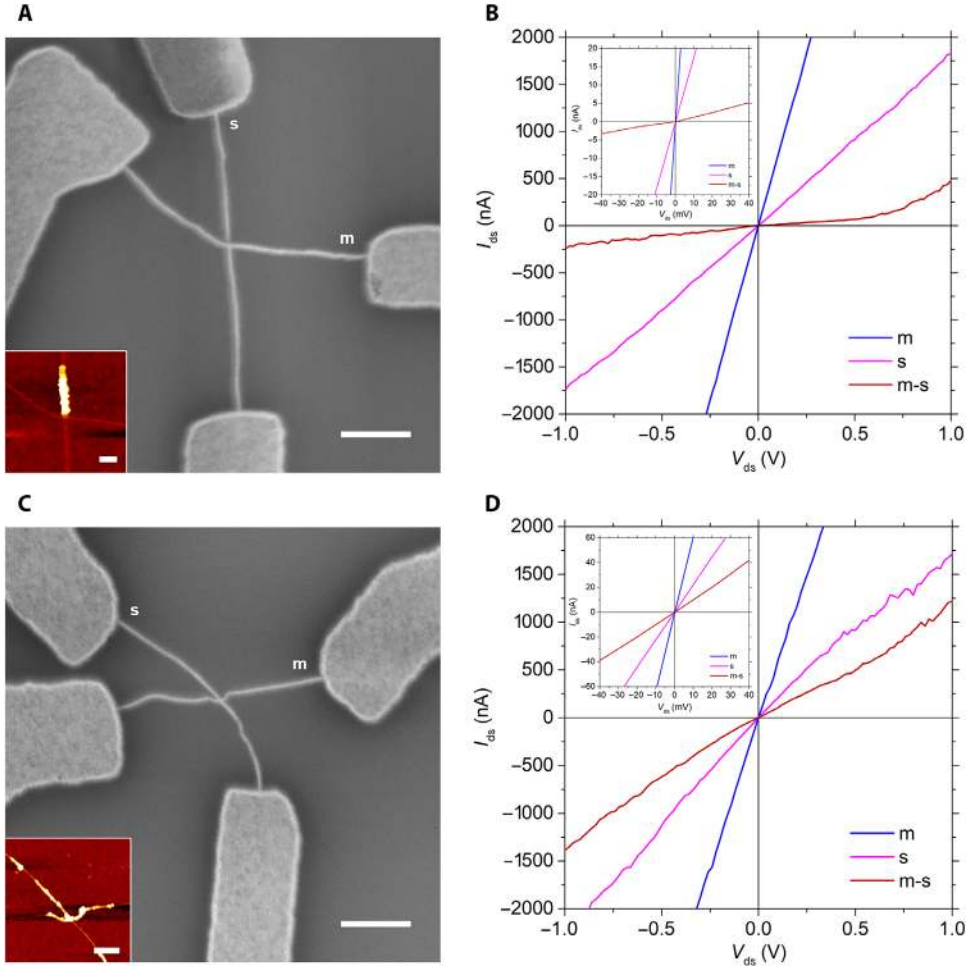

Fig. 5. Layout and performance of SWCNT FETs. (**A** and **C**) SEM images of two representative SWCNT FETs without (A) and with (C) the carbon-welded joint. Scale bars, 1 μm. The inset AFM images show the deposited carbon (white part) on the SWCNTs. Scale bars, 100 and 200 nm, respectively. (**B** and **D**) I_{ds} versus V_{ds} of the device (A) and (C), respectively. Gate voltage V_{gs} = −10 V.

demonstrate great potential for use as transparent electrodes in various flexible electronics.

MATERIALS AND METHODS

Synthesis of SWCNT networks

An injection FCCVD method (fig. S1) (*23*) was used for the synthesis of isolated SWCNT networks with carbon-welded joints. Briefly, a quartz tube reactor with an inner diameter of 46 mm was inserted into a horizontal tubular furnace. A temperature controller was installed to keep the input gases flowing into the reactor through the needlepoint of an injector at a constant temperature. The growth temperature was set to be 1100°C, and the heating zone of the reactor was about 60 cm in length. First, the furnace temperature and the controller temperature were increased to 1100 and 83°C, respectively, under an argon (Ar) atmosphere. Then, 8000 standard cubic centimeters per minute (sccm) of H_2 carrier gas and 11 sccm of C_2H_4 carbon source were introduced, and 4.0 μl min^{-1} of mixed solution [toluene (10 g), ferrocene (0.3 g), and thiophene (0.045 g), acting as a carbon source, catalyst precursor, and growth promoter, respectively] was injected into the reactor by a syringe pump. The SWCNT films with different thicknesses were collected on porous cellulose filter membranes (CA-CN of 0.45-μm-diameter pores, with a typical collection area of 5.5 cm in diameter) installed at the outlet of the flowing gases by changing the collection time. The collection time was 5 to 10 min for TEM, 5 s to 10 min for SEM, and 90 min for 90% *T* samples for TCF. The large-area SWCNT films were collected on porous cellulose filter membranes (CA-CN of 0.45-μm-diameter pores; collection area, 80 mm × 80 mm) for ~100 min using a homemade setup (fig. S5A). After the growth and collection of SWCNTs, the furnace was cooled down to room temperature under the protection of an Ar flow. The bundled SWCNT networks without carbon-welded joints were synthesized, when the flux of H_2 was changed to 4500 sccm, whereas the other experiment parameters were unchanged, with 10 to 30 s collection time for TEM and 90 s collection time for 90% *T* samples.

Characterization

TEMs (JEOL 2010 and Tecnai G2 F20, operated at 200 kV; JEM-ARM200F-G, operated at 80 kV, equipped with a Cs-corrector), a STEM (dark-field)–EELS unit (JEM-ARM200F-B, operated at 200 kV, in STEM mode; Gatan GIF Quantum ER), an SEM unit (FEI XL30 S-FEG, operated at 10 or 1 kV), a micro-Raman spectroscopy unit [Jobin Yvon HR800, excited by 532-, 633-, and 785-nm lasers; we used the following formula (*28*): $\omega = 204\ cm^{-1}\ nm/d + 27\ cm^{-1}$ to calculate the diameter (*d*) of SWCNTs from their RBM Raman peaks (ω)], and an XPS unit (ESCALAB250, operated at 15 kV and 150 W) were used to characterize the structure of the SWCNT networks. For SEM observations, the SWCNT networks were transferred from a porous cellulose filter membrane onto a SiO_2/Si substrate by pressing them together. For TEM observations, the SWCNT networks were transferred from the porous cellulose membrane to a Cu grid on a PET substrate by pressing them together. The *T* of TCFs for 550-nm light was measured by a Varian Cary 5000 UV-vis-NIR instrument, which was also used to obtain the absorption spectrum of the SWCNT film transferred from a porous cellulose filter membrane onto a quartz substrate by pressing them together. As for the Kataura plot used to analyze the Raman spectra and the absorption spectrum, we used the classical Kataura plot by the Maruyama group from a database website (www.photon.t.u-tokyo.ac.jp/~maruyama/kataura/kataura.html), which is able to cover large-diameter SWCNTs. The R_s was measured at least four different points for every TCF by a four-point probe meter (4-probe Tech., RTS-9 with 0.5-mm-diameter probes), and the maximum R_s deviation for specific *T* is below 6% by performing three or four experiments. The theoretical relationship of *T* versus R_s is $T = \exp(-\alpha/(\sigma_{dc,B} R_s))$, where α is the absorption coefficient and $\sigma_{dc,B}$ is the bulk dc conductivity of the film (*31*). Current-brightness-voltage characteristics of the OLEDs without packaging were characterized by Keithley source measurement units (Keithley 2400 and Keithley 2000) with a calibrated silicon photodiode. AFM characterization was performed using a Bruker Innova AFM in tapping mode. The electrical measurements of the SWCNT FETs were performed using a semiconductor analyzer (Agilent B1500A) in ambient air.

SWCNT TCFs

A dry-filtration and transfer process (*13*) was used to obtain SWCNT TCFs on target substrates. The SWCNT film collected on a porous cellulose filter membrane was gently placed on a piece of PET film with the SWCNT film contacting the PET. With gentle stroking, the SWCNT film was easily transferred to PET because of their relatively strong interaction. Ethanol was then dripped onto and spread over the film to densify it. For HNO_3 doping, SWCNT TCFs were immersed in a 67 weight % HNO_3 solution at 50°C for 30 min followed by rinsing with deionized water to remove residual HNO_3. Then, N_2 purging was used to dry the deionized water. An accelerated aging test (250 hours at 60°C and 90% relative humidity) was performed in an environmental chamber (Yiheng, LHS-100CL).

Bending test

A homemade setup was used to perform the bending tests of SWCNT TCF (fig. S6D). For cycling tests, the values of R_s and *T* for SWCNT TCFs were measured every 2000 cycles with a bending angle of 70° and a minimum radius of curvature of 5 mm, and the total bending cycles were 10,000. For the commercial ITO-PET TCF, the sample was measured every 200 cycles, and the total bending cycles were 1000. R_s and *T* of the SWCNT TCF and commercial ITO-PET TCF were measured at bending angles of 45°, 90°, 135°, and 180° (with a corresponding radius of curvature of 3 mm). Because of the limitation of the test setup of SWCNT OLEDs, the bending tests were performed manually. For cycling tests, the luminance of SWCNT OLEDs was measured every 200 cycles with a bending angle of 70° and a minimum radius of curvature of ~4 mm, and the total bending cycles were 800. The luminance of the SWCNT OLEDs was measured at bending angles of 70° and 140° (with a corresponding radius of curvature of ~2 mm).

Thermal stability test

Before heat treatment, the SWCNT samples were transferred from a porous cellulose filter membrane to a Si_3N_4 grid placed on a PET substrate by simple pressing. After the furnace was heated to the target temperature (400°, 500°, 600°, 700°, 750°, or 800°C), the grid was put at the center of the furnace for 30 min in air. Then, the grid was taken out and subjected to TEM observations to check for structural changes in the SWCNT samples.

OLEDs with SWCNT TCF anodes

The structure of the SWCNT OLEDs without packaging is schematically shown in fig. S7A (*44*). About 30 nm of PEDOT:PSS [poly(3,4-ethylenedioxythiophene) polystyrene sulfonate)] was sprayed onto the pristine SWCNT TCF, which was then patterned using the method described earlier (*44*). The patterned SWCNT anodes were loaded into a high vacuum chamber for the thermal deposition of a 3-nm MoO_3 film

(hole injection layer), 166-nm organic films, a 1-nm LiF film (electron injection layer), and 120-nm Al (cathode). The organic films were formed by depositing 80 nm 1,1-bis((di-4-tolylamino)phenyl)cyclohexane (hole transportation layer), two 8-nm bis(2-phenylpyridine)(acetylacetonate) iridium(III)[$Ir(ppy)_2(acac)$] doped with 1,1-bis[4-[*N*,*N*-di(*p*-tolyl)amino] phenyl]cyclohexane and bathophenanthroline (Bphen) (light emission layer), and 70-nm Bphen (electron transport layer). The active area defined by the cathode was 4 mm × 4 mm.

SWCNT FETs

Bottom-gate SWCNT FETs were fabricated on highly doped p-Si substrates with a thermally grown SiO_2 layer (100 nm) as a gate dielectric. The bottom-gate electrode (Ti/Au, 5 nm/50 nm) was deposited by electron beam evaporation after the SiO_2 layer on the back side of the wafer was etched away by reactive ion etching. The SWCNTs were transferred from porous cellulose filter membranes onto the Si substrates by simple pressing. An SEM (1 kV, 3.0 spot size) was used to locate crossed SWCNTs. Electron beam resist poly(methylmethacrylate) was spin-coated over the substrates. Source and drain electrodes (Ti/Au, 5 nm/50 nm) were deposited on the top of the SWCNTs using standard electron beam lithography, electron beam evaporation, and lift-off process. The as-prepared devices were heat-treated for 30 min in Ar at 500° to 550°C. AFM characterization was performed to distinguish the junction types, that is, with or without the carbon-welded joints, by both morphology observations and height measurements.

SUPPLEMENTARY MATERIALS

Supplementary material for this article is available at http://advances.sciencemag.org/cgi/content/full/4/5/eaap9264/DC1

fig. S1. Experimental setup for SWCNT synthesis.
fig. S2. Typical TEM images of different SWCNTs.
fig. S3. Microstructures of isolated SWCNTs with carbon-welded joints.
fig. S4. Thermal and optical characterizations.
fig. S5. Experimental setup for preparing large-area SWCNT films and their characterizations.
fig. S6. Optical, electrical, and mechanical characterizations of SWCNT films.
fig. S7. SWCNT OLEDs.
fig. S8. SWCNT FETs.
table S1. Summary of the performance of pristine or doped SWCNT TCFs.
table S2. Chemical stability of a pristine SWCNT TCF evaluated by an accelerated aging test.
movie S1. Bending test of SWCNT OLED.
Reference (*45*)

REFERENCES AND NOTES

1. D. S. Ginley, H. Hosono, D. C. Paine, *Handbook of Transparent Conductors* (Springer, 2010).
2. D. S. Hecht, A. M. Heintz, R. Lee, L. Hu, B. Moore, C. Cucksey, S. Risser, High conductivity transparent carbon nanotube films deposited from superacid. *Nanotechnology* **22**, 169501 (2011).
3. K. Mustonen, P. Laiho, A. Kaskela, Z. Zhu, O. Reynaud, N. Houbenov, Y. Tian, T. Susi, H. Jiang, A. G. Nasibulin, E. I. Kauppinen, Gas phase synthesis of non-bundled, small diameter single-walled carbon nanotubes with near-armchair chiralities. *Appl. Phys. Lett.* **107**, 013106 (2015).
4. A. Kaskela, P. Laiho, N. Fukaya, K. Mustonen, T. Susi, H. Jiang, N. Houbenov, Y. Ohno, E. I. Kauppinen, Highly individual SWCNTs for high performance thin film electronics. *Carbon* **103**, 228–234 (2016).
5. S. Bae, H. Kim, Y. Lee, X. Xu, J.-S. Park, Y. Zheng, J. Balakrishnan, T. Lei, H. R. Kim, Y. I. Song, Y.-J. Kim, K. S. Kim, B. Özyilmaz, J.-H. Ahn, B. H. Hong, S. Iijima, Roll-to-roll production of 30-inch graphene films for transparent electrodes. *Nat. Nanotechnol.* **5**, 574–578 (2010).
6. J.-Y. Lee, S. T. Connor, Y. Cui, P. Peumans, Solution-processed metal nanowire mesh transparent electrodes. *Nano Lett.* **8**, 689–692 (2008).
7. P.-C. Hsu, S. Wang, H. Wu, V. K. Narasimhan, D. Kong, H. R. Lee, Y. Cui, Performance enhancement of metal nanowire transparent conducting electrodes by mesoscale metal wires. *Nat. Commun.* **4**, 2522 (2013).
8. Y. Xia, K. Sun, J. Ouyang, Solution-processed metallic conducting polymer films as transparent electrode of optoelectronic devices. *Adv. Mater.* **24**, 2436–2440 (2012).
9. C. Feng, K. Liu, J.-S. Wu, L. Liu, J.-S. Cheng, Y. Zhang, Y. Sun, Q. Li, S. Fan, K. Jiang, Flexible, stretchable, transparent conducting films made from superaligned carbon nanotubes. *Adv. Funct. Mater.* **20**, 885–891 (2010).
10. J. Zhang, L. Gao, J. Sun, Y. Liu, Y. Wang, J. Wang, Incorporation of single-walled carbon nanotubes with PEDOT/PSS in DMSO for the production of transparent conducting films. *Diam. Relat. Mater.* **22**, 82–87 (2012).
11. D. S. Hecht, D. Thomas, L. Hu, C. Ladous, T. Lam, Y. Park, G. Irvin, P. Drzaic, Carbon-nanotube film on plastic as transparent electrode for resistive touch screens. *J. Soc. Inf. Disp.* **17**, 941–946 (2009).
12. Z. Wu, Z. Chen, X. Du, J. M. Logan, J. Sippel, M. Nikolou, K. Kamaras, J. R. Reynolds, D. B. Tanner, A. F. Hebard, A. G. Rinzler, Transparent, conductive carbon nanotube films. *Science* **305**, 1273–1276 (2004).
13. A. Kaskela, A. G. Nasibulin, M. Y. Timmermans, B. Aitchison, A. Papadimitratos, Y. Tian, Z. Zhu, H. Jiang, D. P. Brown, A. Zakhidov, E. I. Kauppinen, Aerosol-synthesized SWCNT networks with tunable conductivity and transparency by a dry transfer technique. *Nano Lett.* **10**, 4349–4355 (2010).
14. P.-X. Hou, W.-S. Li, S.-Y. Zhao, G.-X. Li, C. Shi, C. Liu, H.-M. Cheng, Preparation of metallic single-wall carbon nanotubes by selective etching. *ACS Nano* **8**, 7156–7162 (2014).
15. K. Mustonen, P. Laiho, A. Kaskela, T. Susi, A. G. Nasibulin, E. I. Kauppinen, Uncovering the ultimate performance of single-walled carbon nanotube films as transparent conductors. *Appl. Phys. Lett.* **107**, 143113 (2015).
16. D. B. Fraser, H. D. Cook, Highly conductive, transparent films of sputtered $In_{2-x}Sn_xO_{3-y}$. *J. Electrochem. Soc.* **119**, 1368–1374 (1972).
17. S. I. Kim, K. W. Lee, B. B. Sahu, J. G. Han, Flexible OLED fabrication with ITO thin film on polymer substrate. *Jpn. J. Appl. Phys.* **54**, 090301 (2015).
18. O. Reynaud, A. G. Nasibulin, A. S. Anisimov, I. V. Anoshkin, H. Jiang, E. I. Kauppinen, Aerosol feeding of catalyst precursor for CNT synthesis and highly conductive and transparent film fabrication. *Chem. Eng. J.* **255**, 134–140 (2014).
19. N. Fukaya, D. Y. Kim, S. Kishimoto, S. Noda, Y. Ohno, One-step sub-10 μm patterning of carbon-nanotube thin films for transparent conductor applications. *ACS Nano* **8**, 3285–3293 (2014).
20. M. S. Fuhrer, J. Nygård, L. Shih, M. Forero, Y.-G. Yoon, M. S. C. Mazzoni, H. J. Choi, J. Ihm, S. G. Louie, A. Zettl, P. L. McEuen, Crossed nanotube junctions. *Science* **288**, 494–497 (2000).
21. P. N. Nirmalraj, P. E. Lyons, S. De, J. N. Coleman, J. J. Boland, Electrical connectivity in single-walled carbon nanotube networks. *Nano Lett.* **9**, 3890–3895 (2009).
22. W. S. Su, T. C. Leung, C. T. Chan, Work function of single-walled and multiwalled carbon nanotubes: First-principles study. *Phys. Rev. B* **76**, 235413 (2007).
23. T. Saito, S. Ohshima, T. Okazaki, S. Ohmori, M. Yumura, S. Iijima, Selective diameter control of single-walled carbon nanotubes in the gas-phase synthesis. *J. Nanosci. Nanotechnol.* **8**, 6153–6157 (2008).
24. Y. C. Choi, S. C. Lim, Selective oxidation of amorphous carbon layers without damaging embedded single wall carbon nanotube bundles. *Jpn. J. Appl. Phys.* **52**, 115101 (2013).
25. M. Endo, Grow carbon fibers in the vapor phase. *Chemtech* **18**, 568–576 (1988).
26. Z. Lin, X. Gui, Q. Gan, W. Chen, X. Cheng, M. Liu, Y. Zhu, Y. Yang, A. Cao, Z. Tang, In-situ welding carbon nanotubes into a porous solid with super-high compressive strength and fatigue resistance. *Sci. Rep.* **5**, 11336 (2015).
27. Z.-I. Zhang, R. Brydson, Z. Aslam, S. Reddy, A. Brown, A. Westwood, B. Rand, Investigating the structure of non-graphitising carbons using electron energy loss spectroscopy in the transmission electron microscope. *Carbon* **49**, 5049–5063 (2011).
28. J. C. Meyer, M. Paillet, T. Michel, A. Moréac, A. Neumann, G. S. Duesberg, S. Roth, J.-L. Sauvajol, Raman modes of index-identified freestanding single-walled carbon nanotubes. *Phys. Rev. Lett.* **95**, 217401 (2005).
29. W. Ma, L. Song, R. Yang, T. Zhang, Y. Zhao, L. Sun, Y. Ren, D. Liu, L. Liu, J. Shen, Z. Zhang, Y. Xiang, W. Zhou, S. Xie, Directly synthesized strong, highly conducting, transparent single-walled carbon nanotube films. *Nano Lett.* **7**, 2307–2311 (2007).
30. A. A. Green, M. C. Hersam, Colored semitransparent conductive coatings consisting of monodisperse metallic single-walled carbon nanotubes. *Nano Lett.* **8**, 1417–1422 (2008).
31. S. De, P. J. King, P. E. Lyons, U. Khan, J. N. Coleman, Size effects and the problem with percolation in nanostructured transparent conductors. *ACS Nano* **4**, 7064–7072 (2010).
32. S. Bae, S. J. Kim, D. Shin, J.-H. Ahn, B. H. Hong, Towards industrial applications of graphene electrodes. *Phys. Scr.* **2012**, 014024 (2012).
33. E.-X. Ding, H. Jiang, Q. Zhang, Y. Tian, P. Laiho, A. Hussain, Y. Liao, N. Wei, E. I. Kauppinen, Highly conductive and transparent single-walled carbon nanotube thin films from ethanol by floating catalyst chemical vapor deposition. *Nanoscale* **9**, 17601–17609 (2017).
34. D.-W. Shin, J. H. Lee, Y.-H. Kim, S. M. Yu, S.-Y. Park, J.-B. Yoo, A role of HNO_3 on transparent conducting film with single-walled carbon nanotubes. *Nanotechnology* **20**, 475703 (2009).
35. M. Radosavljević, J. Lefebvre, A. T. Johnson, High-field electrical transport and breakdown in bundles of single-wall carbon nanotubes. *Phys. Rev. B* **64**, 241307 (2001).
36. J. Du, S. Pei, L. Ma, H.-M. Cheng, 25th anniversary article: Carbon nanotube- and graphene-based transparent conductive films for optoelectronic devices. *Adv. Mater.* **26**, 1958–1991 (2014).

37. B. Zhang, F. Li, Z. Lin, C. Wu, T. Guo, W. Liu, Y. Su, J. Du, Flexible white organic light-emitting diodes based on single-walled carbon nanotube:poly(3,4-ethylenedioxythiophene)/poly(styrene sulfonate) transparent conducting film. *Jpn. J. Appl. Phys.* **51**, 070204 (2012).
38. E. C.-W. Ou, L. Hu, G. C. R. Raymond, O. K. Soo, J. Pan, Z. Zheng, Y. Park, D. Hecht, G. Irvin, P. Drzaic, G. Gruner, Surface-modified nanotube anodes for high performance organic light-emitting diode. *ACS Nano* **3**, 2258–2264 (2009).
39. C. D. Williams, R. O. Robles, M. Zhang, S. Li, R. H. Baughman, A. A. Zakhidov, Multiwalled carbon nanotube sheets as transparent electrodes in high brightness organic light-emitting diodes. *Appl. Phys. Lett.* **93**, 183506 (2008).
40. Q.-D. Ou, L.-H. Xu, W.-Y. Zhang, Y.-Q. Li, Y.-B. Zhang, X.-D. Zhao, J.-D. Chen, J.-X. Tang, Light outcoupling enhanced flexible organic light-emitting diodes. *Opt. Express* **24**, A674–A681 (2016).
41. W. G. Xie, J. Chen, J. Chen, S. Z. Deng, J. C. She, N. S. Xu, Effect of hydrogen treatment on the field emission of amorphous carbon film. *J. Appl. Phys.* **101**, 084315 (2007).
42. S. Suzuki, C. Bower, Y. Watanabe, O. Zhou, Work functions and valence band states of pristine and Cs-intercalated single-walled carbon nanotube bundles. *Appl. Phys. Lett.* **76**, 4007–4009 (2000).
43. K. A. Ritter, J. W. Lyding, The influence of edge structure on the electronic properties of graphene quantum dots and nanoribbons. *Nat. Mater.* **8**, 235–242 (2009).
44. S. Jia, H. D. Sun, J. H. Du, Z. K. Zhang, D. D. Zhang, L. P. Ma, J. S. Chen, D. G. Ma, H. M. Cheng, W. C. Ren, Graphene oxide/graphene vertical heterostructure electrodes for highly efficient and flexible organic light emitting diodes. *Nanoscale* **8**, 10714–10723 (2016).
45. W. Kim, A. Javey, O. Vermesh, Q. Wang, Y. Li, H. Dai, Hysteresis caused by water molecules in carbon nanotube field-effect transistors. *Nano Lett.* **3**, 193–198 (2003).

Acknowledgments: We thank J. Luan and C. Shi for the preparation setup building, F. Zhang for some of the TEM characterization, B. Tong for help in OLED fabrication and characterization, O. Cretu and Y. Nemoto for help in STEM-EELS characterization, and D. G. Ma, Y. H. Lee, L. C. Yin, H. T. Cong, and C. Zhen for useful discussion. **Funding:** This work was supported by the Ministry of Science and Technology of China (grant 2016YFA0200101), the National Natural Science Foundation of China (grants 51625203, 51532008, 51521091, 51772303, 51572264, 51390473, 51371178, and 51372254), the Chinese Academy of Sciences (grant KGZD-EW-T06), the CAS/SAFEA (Chinese Academy of Sciences/State Administration of Foreign Experts Affairs) International Partnership Program for Creative Research Teams, the Molecular and Thin Film Engineering for Building Integrated Photonics and Process Industry project of the Aalto University Aalto Energy Efficiency Research Programme and the Liaoning BaiQianWan Talents Program. **Author contributions:** S.J., P.-X.H., C.L., and H.-M.C. conceived and designed the experiments. S.J. carried out the sample preparation and most of the characterization. S.J., B.-W.W., and D.-M.S. carried out TCF fabrication. S.J. conducted the characterization of the TCFs. D.-M.T. performed high-resolution Cs-corrected TEM and STEM-EELS characterizations. Q.-X.G., D.-D.Z., S.J., and J.-H.D. carried out the OLED fabrication and characterization. M.-L.C., S.J., and D.-M.S. carried out FET fabrication and most of the characterization. Q.J., S.J., and K.-P.T. performed AFM characterization. S.J., P.-X.H., C.L., H.-M.C., and E.I.K. performed data analysis. S.J., P.-X.H., C.L., and H.-M.C. wrote the manuscript. All authors discussed the results and commented on the manuscript. **Competing interests:** P.-X.H., S.J., C.L., and H.-M.C. are inventors on an international patent related to this work filed by the Institute of Metal Research Chinese Academy of Sciences (WO/2017/219853; 28 December 2017). All other authors declare that they have no competing interests. **Data and materials availability:** All data needed to evaluate the conclusions in the paper are present in the paper and/or the Supplementary Materials. Additional data related to this paper may be requested from the authors.

Submitted 11 September 2017
Accepted 16 March 2018
Published 4 May 2018
10.1126/sciadv.aap9264

Citation: S. Jiang, P.-X. Hou, M.-L. Chen, B.-W. Wang, D.-M. Sun, D.-M. Tang, Q. Jin, Q.-X. Guo, D.-D. Zhang, J.-H. Du, K.-P. Tai, J. Tan, E. I. Kauppinen, C. Liu, H.-M. Cheng, Ultrahigh-performance transparent conductive films of carbon-welded isolated single-wall carbon nanotubes. *Sci. Adv.* **4**, eaap9264 (2018).

Ultrahigh-performance transparent conductive films of carbon-welded isolated single-wall carbon nanotubes

Song Jiang, Peng-Xiang Hou, Mao-Lin Chen, Bing-Wei Wang, Dong-Ming Sun, Dai-Ming Tang, Qun Jin, Qing-Xun Guo, Ding-Dong Zhang, Jin-Hong Du, Kai-Ping Tai, Jun Tan, Esko I. Kauppinen, Chang Liu and Hui-Ming Cheng

Sci Adv **4** (5), eaap9264.
DOI: 10.1126/sciadv.aap9264